Computational Materials Science 102 (2015) 119–125

Contents lists available at ScienceDirect

Computational Materials Science

journal homepage: www.elsevier.com/locate/commatsci

Electronic, structural, and hyperfine properties of pure and Cd-doped hexagonal La_2O_3 semiconductor

D. Richard [a,*], L.A. Errico [a,b], M. Rentería [a]

[a] Departamento de Física and Instituto de Física La Plata (IFLP, CONICET), Facultad de Ciencias Exactas, Universidad Nacional de La Plata, CC 67, (1900) La Plata, Argentina
[b] Universidad Nacional del Noroeste de la Pcia. de Buenos Aires (UNNOBA), Monteagudo 2772, (2700) Pergamino, Argentina

ARTICLE INFO

Article history:
Received 28 November 2014
Received in revised form 6 February 2015
Accepted 11 February 2015
Available online 5 March 2015

Keywords:
Lanthanum oxide
Hyperfine interactions
Electric-field-gradient
DFT calculations
Doped semiconductor
Perturbed angular correlations

ABSTRACT

We present a detailed first-principles study of structural, electronic, and hyperfine properties of pure and Cd-doped lanthanum sesquioxide (La_2O_3) with the hexagonal structure (*A*-phase). We calculated the equilibrium structure, the density of states (DOS), the energy band-gap and, finally, the electric-field-gradient (EFG) tensor at the different atomic sites (La, O, and Cd at substitutional La sites) using different approximations for the exchange and correlation potential. In the case of pure *A*-La_2O_3 our predictions are compared with available experimental data obtained in X-ray Diffraction experiments and Nuclear Quadrupole Resonance and Nuclear Magnetic Resonance spectroscopies. The excellent agreement between theory and experiments gave us a solid base for the study of Cd-doped *A*-La_2O_3. In the case of the doped system, a very good agreement between the predicted and the experimental EFG at the ^{111}Cd sites (obtained in Time-Differential Perturbed γ–γ Angular Correlations experiments) was found. From the comparison of the EFGs obtained at different probe sites we can discuss and elucidate the role played by the electronic structure of the probe atoms, and the structural and electronic modifications induced by the Cd impurity in the La_2O_3 host, on the origin of the EFG.

1. Introduction

Nuclear techniques, such as Mössbauer Spectroscopy (MS), Time-Differential Perturbed γ–γ Angular Correlations (PAC), Nuclear Quadrupole Resonance (NQR), and Nuclear Magnetic Resonance (NMR) are widely used in material science. With these techniques the local environment (at a subnanoscopic scale) around a given probe atom can be elucidated and an accurate knowledge of the structural, electronic, and magnetic properties of a solid is potentially affordable. All these techniques are based on the hyperfine interaction of a probe-nucleus with its surrounding electronic charge distribution [1]. In the case of pure nuclear quadrupole interactions, the electric-field-gradient (EFG) tensor at the probe-nucleus can be determined. Due to the r^{-3} dependence of the EFG from the charge sources, this observable is an extremely sensitive tool for investigating the crystal electronic charge density at a given site.

Recently, we applied electronic structure calculations based on Density Functional Theory (DFT) to the study of the EFG at cationic sites of lanthanide sesquioxides with the cubic bixbyite structure (*C*-Ln_2O_3) [2]. In those systems an accurate description of the electronic structure is a great challenge due to the presence of Ln-4*f* electrons. In that study we showed that the inclusion of an on-site Coulomb repulsion parameter *U* to describe the strong *f*–*f* interactions produce a better description of the crystal structure and the insulating ground state for the entire *C*-Ln_2O_3 series, but this capability of the method does not always guarantee a good prediction of the EFG at Ln sites. The most important discrepancies between the APW+lo prediction and the experimental EFG at the cationic sites of the Ln_2O_3 structures arise in the cases that involve a partially filled Ln-4*f* shell, being the prime example the *C*-Yb_2O_3 case [2].

Lanthanum sesquioxide (La_2O_3) is a semiconductor that has been largely investigated due to its potential application as a high-permittivity material, i.e. as gate insulator in metal–oxide-semiconductor structures [3–5]. It is the only lanthanide oxide with an empty Ln-4*f* shell, and at low temperatures it crystallizes in a simple hexagonal structure (*A*-phase, space group *P*-3*m*1), with a single cationic site. For this reason, a precise (and easy to analyze) experimental characterization of the EFG is potentially reachable.

Over the last years the hyperfine interactions at La and O sites of the *A*-La_2O_3 structure were studied using NQR and NMR techniques [6–9]. *A*-La_2O_3 has also been studied by means of PAC spectroscopy [10,11]. PAC provides a high-resolution determination of the EFG tensor at the site of a probe atom (generally an impurity in the

* Corresponding author. Tel.: +54 221 4246062; fax: +54 221 4252006.
E-mail address: richard@fisica.unlp.edu.ar (D. Richard).

http://dx.doi.org/10.1016/j.commatsci.2015.02.023
0927-0256/

system under study, in the present case ^{111}Cd). The measured EFG may give structural and electronic information of the system that cannot be obtained by other techniques, but the interpretation of such measurements is not straightforward and involves understanding of chemical differences between the probe atom and the ion replaced by the impurity. Additional difficulties (such as the hygroscopic nature of A-La_2O_3) must be considered during the experiment and, afterwards, in the data analysis. The published PAC studies of ^{111}Cd-doped A-La_2O_3 refer to a unique hyperfine interaction. This interaction was assigned (based in the symmetry of the La sites) to ^{111}Cd substitutionally located at the cation sites of the structure [10,11].

From the first-principles point of view, different *ab initio* studies were performed in order to describe different structural or electronic properties of pure A-La_2O_3 [12–20], but neither of them examined the EFG. Considering the fact that the La atom does not involve 4*f* electrons, the A-La_2O_3 system is a unique candidate to study the EFG at La sites without the strong *f*–*f* correlation. In addition, the availability of EFG measurements at the different atomic sites in pure A-La_2O_3, and at the Cd-impurity site in ^{111}Cd-doped A-La_2O_3 turns this oxide in a very interesting system to be investigated by means of first-principles methods such as the APW+lo method, one of the state-of-the-art and most accurate tool for the calculation of the EFG tensor.

In the present work we present an APW+lo study of the electronic, structural, and hyperfine properties of pure A-La_2O_3, focusing on the EFG. After that, we analyzed the Cd-doped system. The goal is not only to reproduce the experimental results but also to elucidate the structural and electronic modifications induced in the host by the presence of the impurity and to understand the origin of the EFG tensor.

The paper is organized as follows. In Section 2 we outline the way we applied the APW+lo method to the study of pure and Cd-doped A-La_2O_3 and, in Section 3, we present and discuss the obtained results. In all cases the theoretical predictions are compared to the existing experimental data in the literature. Finally, in Section 4, we present our conclusions.

2. Method of calculation

A-La_2O_3 crystallizes in the hexagonal structure of the rare earth sesquioxides (space group P-3m). The unit cell contains one formula unit with the two equivalent La atoms located at positions 2*d*: ±(1/3,2/3,u). Two nonequivalent sites for the oxygen atoms (O1 and O2 in the following) characterize the structure. The O1 are located at positions 1*a* (at the origin) and O2 are at 2*d:* ±(1/3,2/3, v,O2) (see Fig. 1(a)). The experimentally determined internal and lattice parameters are u = 0.245(5), v = 0.645(5), a = 3.9373 Å, c = 6.1299 Å, respectively [21]. Each La atom is coordinated with seven oxygen nearest neighbours (ONN, see Fig. 1(b)).

As mentioned before, the experimental hyperfine techniques whose results will be discussed in this work allow the determination of the EFG tensor, which is a fingerprint of the asymmetry of the electronic charge density near and at the probe nucleus. The EFG is a rank 2 traceless symmetric tensor whose components, denoted by V_{ij}, are defined by the second derivative (with respect to the spatial coordinates) of the Coulomb potential $V(\boldsymbol{r})$ created by the charge density surrounding a given probe-nucleus. In the principal axis system the three diagonal components of the EFG tensor are labeled according to the conventional choice $|V_{xx}| < |V_{yy}| < |V_{zz}|$. Hence, V_{zz} is the largest eigenvalue of the EFG tensor. The measured magnitudes (in the case of the experiments discussed here) are the nuclear quadrupole coupling constant ν_Q, related to V_{zz} by [1]:

$$\nu_Q = \frac{eQV_{zz}}{h} \tag{1}$$

and the asymmetry parameter $\eta = (V_{xx} - V_{yy})/V_{zz}$. Q is the nuclear quadrupole moment of the sensitive states of ^{111}Cd (PAC probe) and ^{139}La, and ^{17}O (MNR, NQR probes). From the symmetry of the La, O1, and O2 sites, which present axial symmetry, the observed/calculated quadrupole interactions should have $\eta = 0$, and V_{zz} is expected to be oriented along the [0, 0, 1] direction.

The calculations were performed with the WIEN2 k implementation of the APW+lo method [22]. The exchange and correlation effects were treated using both the local density approximation (LDA) [23] and the Wu and Cohen parameterization of the generalized gradient approximation (WC-GGA) [24]. Also, we employed the LDA approximation plus the Hubbard U term (LDA+U approach), in the self-interaction-corrected scheme [25,26]. To this purpose we took U = 10.9 eV (0.8 Ry) for the La-4*f* orbitals [2]. The product of the smallest muffin-tin radius (R_{MT}) and the largest wavenumber of the basis set (K_{max}) was fixed to 7. Integration in the reciprocal space was performed using the tetrahedron method, taking up to 100 k points in the first Brillouin zone. The muffin-tin radii used for cations and O atoms were 1.06 and 1.00 Å, respectively.

For the pure A-La_2O_3 system we used the experimental lattice and internal parameters as starting values. We first calculated the electronic band structure and the density of states (DOS) of the pure compound by using the LDA and the WC-GGA approximations. Due to the well-known deficiency of the LDA and WC-GGA to predict the energy band-gaps of semiconductors [27], we additionally used the modified version of the Becke and Johnson exchange potential proposed by Tran and Blaha (TB–mBJ method), which in general predicts very accurate energy band-gaps in most semiconductors and insulators [19,28–30]. To determine the equilibrium structural properties of the system we fitted the Birch-Murnaghan equation of state (EOS) [31] to the calculated energy vs. volume data. Also, we predicted the equilibrium atomic positions, i.e., we obtained the u and v parameters predicted by the *ab initio* calcula-

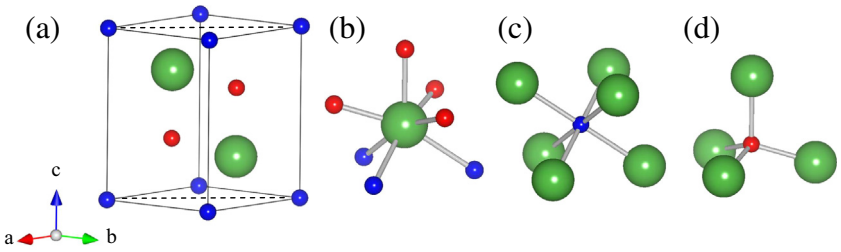

Fig. 1. (a) A-La_2O_3 unit cell, and coordination of the atomic sites of (b) La, (c) O1, and (d) O2 atoms. The big green spheres represent La atoms, the small blue spheres represent O1 atoms, and the small red spheres represent O2 atoms. In the dashed lines are used to indicate the (1 1 0) plane. In the three O1 atoms are the more distant to the La atom, while the three non azimuthal O2 atoms are the nearest. (For interpretation of the references to colour in this figure legend, the reader is referred to the web version of this article.)

tions. To do this, we calculated self-consistently the forces on the ions, and displaced the atoms until the forces were below a tolerance value of 0.025 eV/Å. The diagonal elements of the EFG tensor were calculated directly from the V_{2M} harmonic coefficients of the potential [32,33] in each step of the self-consistent calculation.

In order to study by first-principles the Cd-doped A-La_2O_3 system, we considered a supercell of dimension $2a \times 2a \times 2c$ and we replaced a La atom by a Cd atom (dilution 1:16). This leads to an ordered compound, $La_{1.875}Cd_{0.125}O_3$, with 6.25 at.% cationic doping, where the Cd atoms are at about 8 Å from each other. This distance has shown to be sufficient to avoid undesired significant Cd–Cd interaction, which is necessary to simulate the dilution of the Cd impurity (ppm) in the PAC samples [2,34,35].

3. Results and discussion

3.1. Pure crystal

The electronic band structure of pure A-La_2O_3 obtained with the LDA approximation is presented in Fig. 2. Both LDA and WC-GGA calculations predict the correct semiconducting nature of A-La_2O_3 with a direct energy band-gap of 3.8 eV between the valence and conduction bands (VB and CB, respectively). This band-gap is about 1.7 eV smaller than the experimental value [36]. In this respect, other authors have predicted that the energy band-gap is indirect by using different first-principles methods, with values between 3.6 eV and 3.85 eV [14,19,20]. In Fig. 3(a) we show the total DOS calculated with the LDA approximation. The contributions of the La and O atoms are presented in the atom-projected partial density of states (PDOS) of Fig. 3(b) and (c), respectively. According to these DOSs, the VB is dominated by O-2p states, with a smaller contribution of La d orbitals. The CB has a prevailing La-4f character, with an additional La-5d contribution. This behaviour is in agreement with the mainly ionic character of this sesquioxide, with some degree of covalent bonding between cations and oxygen atoms. LDA and WC-GGA predict similar DOSs. The obtained band structure and DOSs are in very good agreement with previous theoretical calculations in A-La_2O_3 and other isostructural sesquioxides using different first-principles methods [13–15,17–20]. In the present work, to avoid the use of empirical factors and extra hypothesis we utilized the TB–mBJ approximation for the exchange and correlation potential to explore the band-gap correction. In Fig. 3(d)–(f) we show the total DOS and the relevant atom-projected PDOS calculated using the TB–mBJ method. As can be seen, the overall band structures are similar to those obtained by LDA, with some minor changes. In this respect, we can observe that TB–mBJ predicts a narrower VB compared to that predicted by LDA (the energy width of the VB decreases from 2.8 eV to 2.5 eV), and predicts a larger energy band-gap of 4.7 eV, which is in better agreement with the experimental band-gap value of 5.5 eV [36].

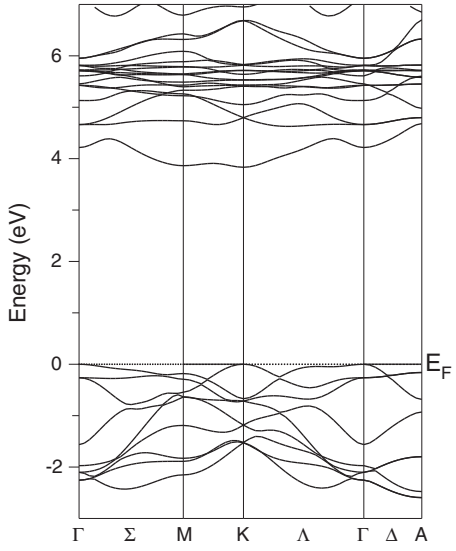

Fig. 2. Calculated band structure for pure A-La_2O_3 predicted by the LDA approximation. Zero energy is at the Fermi level (E_F), denoted by a dotted horizontal line.

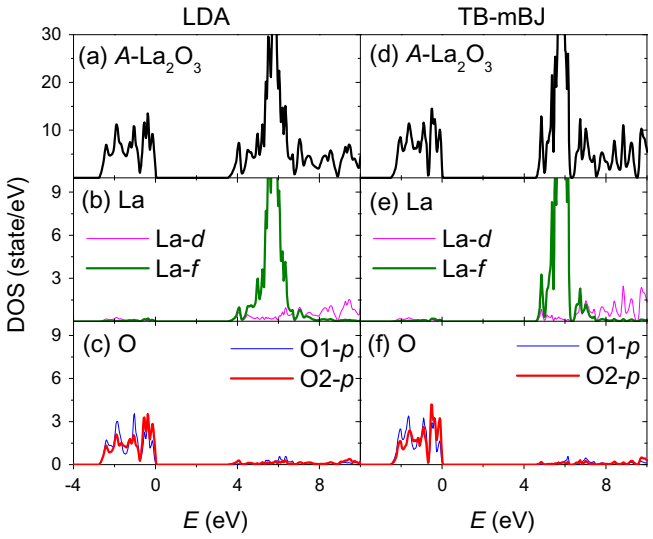

Fig. 3. Calculated total and atom-projected partial density of states (DOS) for pure A-La_2O_3 predicted by (a)-(c) the LDA approximation and (d)-(f) the TB–mBJ method. For La and O atoms the most relevant contributions are presented. Different scales were used on the y axes to optimize visibility in all graphs. Energies refer to the highest occupied state.

In Fig. 4(a) we present a projection of the LDA prediction for the total electron density $\rho(\boldsymbol{r})$ at the (1 1 0) plane, which contains the La, O1, and O2 atoms on the same plane. According to this figure, there is a very small degree of covalence between La and O atoms, confirming the mainly ionic character of the La–O bonds. In Fig. 4(b) we plot the electron density of the valence states $\rho^{val}(\boldsymbol{r})$ in the same plane, which shows the dominant contribution of the O-2p valence orbitals on the total electron density and, at the same time, shows the small contribution of the La-states on this range of energies. Also, in contrast to Fig. 4(a), the scale used in Fig. 4(b) helps to visualize the weak covalent bonding between the La and the three different O atoms through the overlapping of their orbitals, according to their different La–O bond-lengths: when the distance between La and O is shorter (see Fig. 1(b)), the bond-strength is larger.

In order to determine the equilibrium lattice parameters a_0 and c_0, we first studied the energy E as a function of the c/a ratio. By doing this, we obtained that the c/a ratio that minimizes E does not differ from the experimental ratio (for both LDA and WC-GGA, a_0/c_0 and a_{exp}/c_{exp} differ in less than 0.2%). So, we fixed the c/a ratio at its experimental value and we calculated E as a function of the unit cell volume V. Then, we determined the equilibrium structural properties, i.e., the equilibrium lattice parameters a_0 and c_0, and the bulk modulus B and its derivative with respect to pressure B', by fitting the Birch-Murnaghan EOS to the $E(V)$ data. In Table 1 we present the corresponding predictions and we compare them with the experimental values. Notice that both approximations predict a_0 and c_0 values that are below the experimental a_{exp} and c_{exp} ones (1.7% below for LDA and 0.9% for WC-GGA), which is within the scope of the calculation method [38]. Our predicted equilibrium structure is in very good

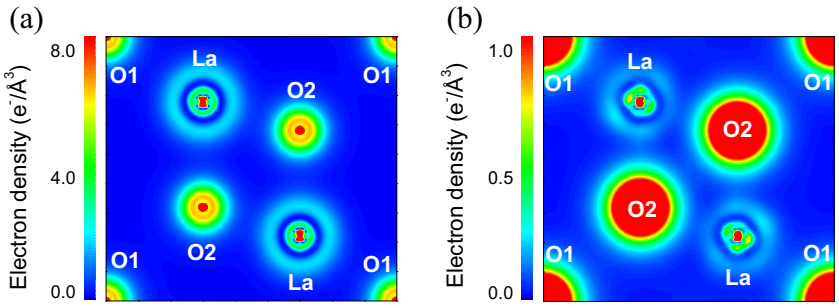

Fig. 4. (a) Total electron density $\rho(\mathbf{r})$ and (b) valence electron density $\rho^{val}(\mathbf{r})$ in the (1 1 0) plane for pure A-La_2O_3. Different scales were used to optimize visibility in each graph.

Table 1
Experimental and equilibrium lattice parameters a_0 and c_0, bulk modulus B, and its derivative B' of pure A-La_2O_3 obtained from the Birch-Murghanan EOS fit in the LDA and WC-GGA approximations.

	a_0 (Å)	c_0 (Å)	B (GPa)	B'
LDA	3.871	6.026	162	5.6
WC-GGA	3.902	6.075	149	6.3
Exp.	3.9373 [21]	6.1299 [21]	113 [37]	6.0 [37]

agreement with previously reported DFT-based calculations for this system [14,17,18,20]. The predictions for B are about 40% larger than the experimental value, and the predictions for B' are in good agreement with the experimental ones (see Table 1). At this point it is important to mention that such differences between the predictions and the experimental value for B could be understand from the fact that the experiment (see Ref. [37]) was done assuming an isotropic compressional strain over the sample and not considering its dependence on temperature and, more decisive, on the porosity of the samples [39,40]. If we considered the measurements of B performed in other hexagonal lanthanide sesquioxides, we observe that B can reach values up to 230 GPa [37,41–47]. So, we consider that our predictions for B comply with the overall experimental measurements in the lanthanide sesquioxides with the A-phase.

Later, we determined the equilibrium u and v parameters, considering the lattice parameters a_{exp} and c_{exp}, and also the predicted a_0 and c_0. In both cases, using the LDA and WC-GGA approximations, the final values for u and v are practically equal to their experimental values, being the differences between theory and experiments smaller than 1%.

In Table 2 we present the predictions for the largest component of the EFG tensor, V_{zz}, at each atomic site of pure A-La_2O_3, considering both the experimental and the equilibrium structures. We observe that, for both approximations, the calculated V_{zz} values at La sites (V_{zz}^{La}) are sensitive to the change in the lattice parameters. In this sense, LDA and WC-GGA approximations predict increments in V_{zz}^{La} of 17% (LDA) and 6% (WC-GGA) when the lattice parameters decrease in less than 2% (see Tables 1 and 2). Therefore, we consider that these dispersions give an estimation of the error bar in the EFG calculations due to the uncertainty in the crystal structure.

Table 2
Theoretical and experimental values for the largest principal component V_{zz} (in units of 10^{21} V/m^2) of the EFG tensor at the atomic sites of pure A-La_2O_3. The signs of the experimentally determined V_{zz} are unknown. Experimental V_{zz} values were obtained from the experimentally determined nuclear quadrupole coupling constant ν_Q, using eq. 1 and Q (^{139}La) = +0.20(1) b and Q(^{17}O) = −0.02578 b (from Ref. 48). In all cases, η^{exp} = 0.00.

	a, c	V_{zz}^{La}	V_{zz}^{O1}	V_{zz}^{O2}
LDA	Experimental	11.3	−0.7	0.9
	Equilibrium	13.2	−0.7	1.1
WC-GGA	Experimental	11.7	−0.8	1.0
	Equilibrium	12.4	−0.8	1.1
Experimental	T = 296 K	12.1(6) [6]		
	T = 77 K	12.32 [7]		
	T = 296 K		<2.21 [8]	<3.53 [8]
	T = 973 K			≈0.7 [9]

Finally, we applied the LDA+U formalism. By doing this, the empty La-f band showed in the DOS predicted by LDA (see Fig. 3(b)) is shifted to higher energies, 10 eV above the valence band maximum, in a similar way to that previously showed for the cubic C-La_2O_3 phase [2]. With respect to the EFG at the La site, this approach does not introduce significant changes in the predicted V_{zz}^{La} value (e.g., using the experimental lattice parameters, LDA+U predicts $V_{zz}^{La} = 12.6 \times 10^{21}$ V/m^2 while LDA predicts $V_{zz}^{La} = 11.3 \times 10^{21}$ V/m^2, being their difference in the order of the precision limit of the calculation), showing that the energy-position of the unfilled states does not affect the EFG.

Among the experimental studies of the hyperfine interactions in pure A-La_2O_3, NQR and NMR techniques allow very accurate determinations of the EFG at the La site. It is important to mention that the EFG does not change significantly from 77 K to room temperature [6,7]. When we compare our predictions for the EFG (obtained using 0 K calculations) with the measured V_{zz}^{La} values we obtain an excellent agreement between theory and experiment (see Table 2). In the case of the EFG at the O sites, different NMR studies with ^{17}O as probe provided estimated values for the EFG at both oxygen sites (V_{zz}^{O1} and V_{zz}^{O2} values are listed in Table 2) [8,9]. In this respect, the LDA and WC-GGA predictions are in agreement with the experimental upper estimations reported in Ref. [8], and in good agreement with the value for V_{zz}^{O2} obtained from Ref. [9].

In order to investigate the origin of the EFG at each atomic site, we decomposed the non-spherical electron density of the valence electrons within the respective R_{MT} sphere according to the different orbital symmetries. For O1 and O2 sites, the EFG is entirely due to the O-2p orbitals. On the other hand, at the La site the p contribution to V_{zz} dominates over the d contribution (more than 80% of V_{zz}^{La} is due to the La-p contribution). This result can be understood from the fact that the first node of the p wavefunction is at much shorter distance than the one of the d wavefunction [32]. In all cases, the mixed contributions to the EFG (s-d, s-p, and p-f) are practically negligible.

3.2. Cd-doped A-La_2O_3

To study Cd-doped A-La_2O_3 we replaced a La atom by a Cd atom in the $2a \times 2a \times 2c$ supercell, and we analyzed the structural and electronic changes induced by the Cd impurity in the electronic and structural properties of the semiconducting host. In this

regard, we followed the same procedure described previously for pure A-La_2O_3, fixing the lattice parameters at the experimental values a_{exp} and c_{exp}. We took this choice because in the real samples the impurity dilution is extremely low (ppm) and will not produce significant changes in the unit cell volume.

Since the substitutional Cd^{2+} in $La_2^{3+}O_3^{2-}$ has a nominal single-acceptor character, we studied two different charge states for the impurity-host system: that coming from the substitution of a La atom by a Cd atom (*neutral cell*), and that with the addition of an extra electron to the supercell (*charged cell*). For the latter, the negative charge excess was compensated with a positive homogeneous background. For both charge states, the presence of the Cd impurity produces non-negligible forces on its ONNs. Hence, we determined the equilibrium atomic positions. To do this we allowed the displacement of all the atoms in the supercell preserving the point group symmetry of the atomic sites, until the Hellmann–Feynman forces on the atoms were below the tolerance value of 0.025 eV/Å (*relaxed structure*).

The calculated electronic band structure obtained with the LDA approximation for the relaxed structure of the neutral cell is shown in Fig. 5. A very similar result was obtained using WC-GGA. Compared with the pure A-La_2O_3 band structure (Fig. 2), the Cd impurity induces the appearance of an impurity level near the VB maximum, which is intersected by the Fermi level. In Fig. 6(a), the corresponding DOS for the Cd-doped system is presented. As can be seen, this total DOS is similar to that of the pure compound: a valence band dominated by the O-2p states is separated by about 4.0 eV from the conduction band, which is mainly due to the La-4f and La-4d states. The Cd impurity induces the appearance of the acceptor states near the VB maximum, at the Fermi energy E_F (see the DOS plots in Fig. 6, on the right). It can be seen that these states form a narrow band, where O-p states fully overlap with Cd-d states, with a contribution of La states. For the neutral cell the system is p-type metallic, and for the charged cell these acceptor states are filled and the resulting system recovers the semiconducting nature of the host. The integration of the DOS in the unfilled energy region of the VB gives a value of 0.9 electrons, in agreement with the nominal single-acceptor character of the impurity. As can be deduced from Fig. 6(c), the electrons that fill the acceptor states when the impurity level is ionized are spatially located mainly at the oxygen atomic spheres and only 5% of this

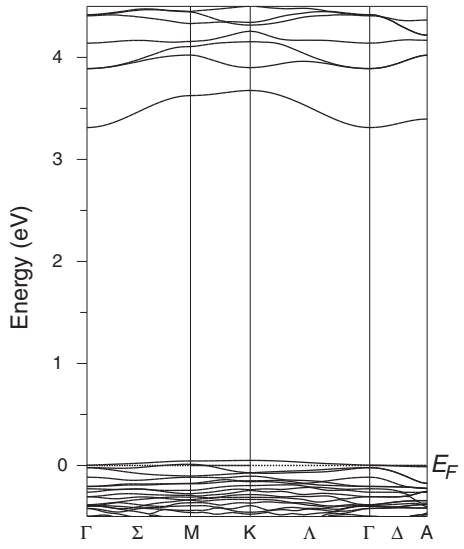

Fig. 5. Calculated band structure for Cd-doped A-La_2O_3 predicted by the LDA approximation (neutral cell). Zero energy is at the Fermi level (E_F), denoted by a dotted horizontal line.

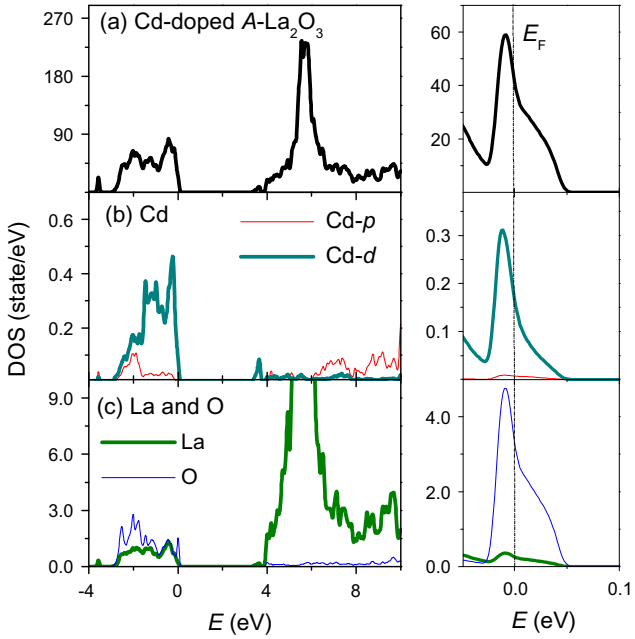

Fig. 6. Calculated (a) total and (b-c) atom-projected partial DOS for Cd-doped A-La_2O_3 predicted by the LDA approximation (neutral cell). On the right, the respective magnifications of the DOS near E_F. For the Cd atom the most relevant contributions are presented in (b). Different scales were used on the y axes to optimize visibility in all graphs.

(extra) charge is at the Cd and La atomic spheres. In this sense, by looking at the electron density $\rho(\boldsymbol{r})$ it is possible to investigate the spatial distribution of this effect. In Fig. 7(a) the projection of $\rho(\boldsymbol{r})$ over the (1 1 0) plane is shown, where the position of the Cd atom in the supercell can be identified. This figure shows that the La and O-states are mostly localized at their atomic spheres, with practically no hybridization with the Cd atom. The electron density $\rho^{imp}(\boldsymbol{r})$ corresponding to the energy range 0–0.05 eV of the impurity acceptor states (see Fig. 6) can be projected on the same plane, as done in Fig. 7(b). This figure shows the contribution of the Cd's ONN to these acceptor states, and gives us a direct description of the localization of the additional electron that ionizes the acceptor states in the charged supercell. As can be seen, while more distant from the Cd impurity the oxygen atom is, the weaker is its contribution to $\rho^{imp}(\boldsymbol{r})$, and the La states are practically absent.

In Table 3 we present the Cd-ONN distances for the unrelaxed and relaxed equilibrium structures, and for the two charge states considered. When we allow the structure to relax, four of the seven ONN atoms (those that are closest to the Cd site) move inward. Three of these Cd-ONN bond lengths are reduced in about 8% with respect to the un-relaxed Cd-ONN bond lengths, while for the fourth ONN the reduction is in the order of 3%. The remaining three ONNs move outward, being their changes in the bond-lengths in the order of 15–20% of the corresponding un-relaxed Cd-ONN bond-lengths. The predicted Cd-ONN distances are in quite good agreement with those calculated considering the empirical ionic radii [49] for the different Cd and O coordination in the A-La_2O_3 structure, i.e., considering the sevenfold coordinated Cd atom, and the sixfold and fourfold coordinated O1 and O2 atoms, respectively. The summation of the respective ionic radii gives 2.43 Å for Cd–O1 and 2.41 Å for Cd–O2 bond-lengths, which are in the order of the obtained mean Cd–ONN distances (see Table 3). It is important to note that the equilibrium relaxed structures are almost independent of the charge state of the supercell.

Concerning the EFG at the Cd site, in Table 3 we present the LDA and WC-GGA predictions. Similar results were obtained using the

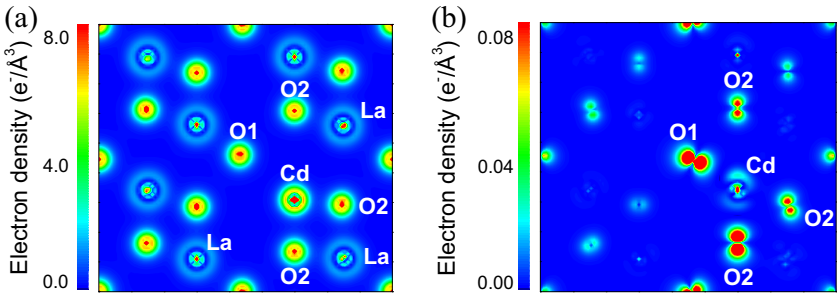

Fig. 7. (a) Total electron density $\rho(\mathbf{r})$ and (b) impurity acceptor states electron density $\rho^{imp}(\mathbf{r})$ in the (1 1 0) plane for Cd-doped A-La_2O_3. Different scales were used to optimize visibility in each graph.

Table 3
Theoretical predictions for Cd-ONN distances (in Å) and the largest principal component V_{zz} (in units of 10^{21} V/m^2) of the EFG tensor at the Cd sites in Cd-doped A-La_2O_3. The seven d(Cd-ONN) distance values are listed indicating their multiplicity in brackets. The three more distant Cd's ONN are O1-type, while the rest are O2-type (see Fig. 1(b)). The sign of the experimentally determined V_{zz} is unknown. The experimental V_{zz} value was obtained from the experimentally determined nuclear quadrupole coupling constant ν_Q, using Eq. 1 and Q(^{111}Cd, I = +5/2) = +0.83(13) b [48]. In all cases, η = 0.00.

Structure	Charge state	Approx.	d (Cd–ONN)	V_{zz}^{Cd}
Unrelaxed	Neutral	LDA	2.37 [3], 2.45 [1], 2.72 [3]	3.9
		WC-GGA		4.0
	Charged	LDA		4.0
		WC-GGA		4.1
Relaxed	Neutral	LDA	2.19 [3], 2.38 [1], 3.27 [3]	13.1
		WC-GGA	2.21 [3], 2.44 [1], 3.16 [3]	13.4
	Charged	LDA	2.21 [3], 2.37 [1], 3.20 [3]	11.3
		WC-GGA	2.22 [3], 2.42 [1], 3.13 [3]	12.2
Experimental (12 K < T < 296 K)				13.9(1) [11]

LDA+U approach. As can be seen, for the unrelaxed structure the magnitude of V_{zz}^{Cd} practically does not depend on the charge state of the supercell (the EFG is calculated for the two charge states considered at the same atomic positions in both cases). When the relaxation of the structure is allowed, it is observed a drastic change in the magnitude of V_{zz} at the Cd site for both charge states (from 4×10^{21} V/m^2 in the case of the unrelaxed structures to about 13×10^{21} V/m^2 for relaxed structures, see Table 3), showing that the EFG at this site strongly depends on the Cd's ONN positions. In the case of these relaxed structures the predicted V_{zz}^{Cd} is slightly different depending on the charge state of the supercell (the V_{zz}^{Cd} value obtained in the relaxed structure of the charged cell is 10% smaller than those obtained at the relaxed structure of the neutral cell). Since the EFG strongly depends on the Cd-ONN distances and different charge states produce slightly different equilibrium structures, it is interesting to separate the electronic and structural effects. In order to do that, we have taken the equilibrium structure of the neutral cell of Cd-doped A-La_2O_3 obtained in the LDA calculations and performed calculations adding one electron to the system without relaxing the structure. Interestingly, we found that the EFG is nearly independent of the charge state of the impurity. For the relaxed structure of the neutral cell, $V_{zz}^{Cd} = 13.1 \times 10^{21}$ V/m^2 (see Table 3), and when the extra electron is added maintaining fixed the structure we obtain $V_{zz}^{Cd} = 12.9 \times 10^{21}$ V/m^2, a value that practically does not differ from the previous one. However, if we allow the charged structure to relax we obtain $V_{zz}^{Cd} = 11.3 \times 10^{21}$ V/m^2 (see Table 3). These results show that the fraction of the additional electron that ends at the Cd muffin-tin sphere (around 5%, as mentioned above) is nearly spherical and therefore it does not contributes to the EFG at this site. Then, V_{zz}^{Cd} is primarily due to the local structure the probe observes.

For both charge states, the EFG at the Cd site is mainly originated by Cd-p orbitals, being their contribution to the total V_{zz}^{Cd} value of about 80%. This result has also been observed in other binary oxides doped with Cd [34,35]. The observed weak dependence of V_{zz}^{Cd} with the charge state of the cell is due to a simultaneous variation in the contributions p and d: when the acceptor states are filled both contributions to V_{zz}^{Cd} decrease.

Our predictions for V_{zz}^{Cd} in Cd-doped A-La_2O_3 are in very good agreement with the low temperature PAC measurements reported in the literature [10,11]. The difference between predictions and measurements depends on the approximation and charge state considered, but is in the order of 10% for V_{zz}^{Cd} (see Table 3). If we take into account the previously discussed precision of the calculation method, we conclude that both neutral and charged states of the considered supercells provide a reliable prediction of the EFG tensor at impurity sites in the ^{111}Cd-doped A-La_2O_3 samples used in PAC experiments.

4. Conclusions

We have performed an *ab initio* study of the electronic, structural, and hyperfine properties of pure and Cd-doped A-La_2O_3 using the APW+lo method.

As witnessed by the calculated DOSs, for both systems the valence band has mainly O-2p character, while the conduction band is composed mainly by La-4f and La-d states. The electron density projections complement these predictions, showing the strongly ionic character of the compound, with a minor covalent bonding between the La and the O atoms. These results are in agreement with those coming from other first-principles studies in La_2O_3 and other isostructural sesquioxides. We also determined the equilibrium structural properties using the Birch-Murnaghan EOS in the pure system, obtaining a general good agreement with the experimental values.

In the case of the Cd-doped system, the impurity induces the appearance of acceptor states at E_F. Therefore, we studied two possible charge states for the supercell, which correspond to those unoccupied (neutral cell) and fully occupied (charged cell) impurity states.

Concerning the EFG tensor, our APW+lo calculations successfully predict the experimental values. For pure A-La_2O_3 the predictions for V_{zz} at La site are in excellent agreement with the experimental results, and the predictions for V_{zz} at O1 and O2 sites are in agreement with their experimental upper estimates. For Cd-doped A-La_2O_3, the impurity induces significant structural distortions in the semiconducting host. These structural distortions are fundamental for a correct prediction of the EFG at the Cd site.

The APW+lo calculations considering the relaxed structures are in very good agreement with the PAC measurements, but we cannot determine the exact charge state of the cell due to the precision limit of the calculation. For both the pure and Cd-doped systems the EFG has a dominating *p*-type contribution.

Finally, our APW+lo calculations showed that the electron that fills the acceptor states is mostly localized at the Cd's ONNs, and produces an indirect change of the EFG at the Cd site through slight modifications of the ONN positions.

Acknowledgements

This work was partially supported by Consejo Nacional de Investigaciones Científicas Técnicas (CONICET) under Project No. PIP 0002. The research made use of the HP-Parallel-Computing Bose Cluster, and the computational facilities of the Physics of Impurities in Condensed Matter group, at Instituto de Física La Plata (IFLP) and Departamento de Física (UNLP).

References

[1] G. Schatz, A. Weidinger, Nuclear Condensed Matter Physics – Nuclear Methods and Applications, John Wiley & Sons, Chichester England, 1996. p. 63.
[2] D. Richard, E.L. Muñoz, M. Rentería, L.A. Errico, A. Svane, N.E. Christensen, Phys. Rev. B 88 (2013) 165206.
[3] P.W. Peacock, J. Robertson, J. Appl. Phys. 92 (2012) 4712.
[4] S. Ohmi, C. Kobayashi, I. Kashiwagi, C. Ohshima, H. Ishiwara, H. Iwai, J. Electrochem. Soc. 150 (2003) 134.
[5] K. Kakushima, K. Tsutsui, S. Ohmi, P. Ahmet, V. Ramgopal, Top. Appl. Phys. 106 (2007) 345.
[6] T.J. Bastow, Solid State NMR 3 (1994) 17.
[7] G.K. Semin, Russ. J. of Phys. Chem. 81 (2007) 38.
[8] T.J. Bastow, S.N. Stuart, Chem. Phys. 143 (1990) 459.
[9] F. Ali, M.E. Smith, S. Steuernagel, H.J. Whitfield, J. Mater. Chem. 6 (1996) 261.
[10] D. Lupascu, J. Albohn, J. Shitu, A. Bartos, K. Królas, M. Uhrmacher, K.P. Lieb, Hyp. Interact. 80 (1993) 959.
[11] D. Lupascu, S. Habenicht, K.P. Lieb, M. Neubauer, M. Uhrmacher, T. Wenzel, Phys. Rev. B 54 (1996) 871.
[12] N. Hirosaki, S. Ogata, C. Kocer, J. Alloys Comp. 351 (2003) 31.
[13] L. Marsella, V. Fiorentini, Phys. Rev. B 69 (2004) 172103.
[14] M. Mikami, S. Nakamura, J. Alloys Comp. 408 (2006) 687.
[15] N. Singh, S.M. Saini, T. Nautiyal, S. Auluck, J. Appl. Phys. 100 (2006) 083525.
[16] H. Jiang, R.I. Gomez-Abal, P. Rinke, M. Scheffler, Phys. Rev. Lett. 102 (2009) 126403.
[17] M. Rahm, N.V. Skorodumova, Phys. Rev. B 80 (2009) 104105.
[18] B. Xu, V.R. Cooper, D.J. Singh, Y.P. Feng, Phys. Rev. B 83 (2011) 064115.
[19] D.J. Singh, Phys. Rev. B 82 (2010) 205102.
[20] C. Chen, J. Xie, S. Chen, Y. Li, Can. J. Phys. 91 (2013) 801.
[21] R.W.G. Wyckoff, Crystal Structures, vol. 2, Wyley, New York, 1964.
[22] P. Blaha, K. Schwarz, G. Madsen, D. Kvasnicka, J. Luitz, WIEN2k: An Augmented Plane Wave+Local Orbitals Program for Calculating Crystal Properties, Vienna University of Technology, Vienna, 2012.
[23] J.P. Perdew, Y. Wang, Phys. Rev. B 45 (1992) 13244.
[24] Z. Wu, R.E. Cohen, Phys. Rev. B 73 (2006) 235116.
[25] V.I. Anisimov, J. Zaanen, O.K. Andersen, Phys. Rev. B 44 (1991) 943.
[26] V.I. Anisimov, I.V. Solovyev, M.A. Korotin, M.T. Czyzyk, G.A. Sawatzky, Phys. Rev. 48 (1993) 16929.
[27] J.P. Perdew, Int. J. Quantum Chem. 28 (1985) 497. 30 (1986) 451(E).
[28] F. Tran, P. Blaha, Phys. Rev. Lett. 102 (2009) 226401.
[29] D. Koller, F. Tran, P. Blaha, Phys. Rev. B 85 (2012) 155109.
[30] J.A. Camargo-Martínez, R. Baquero, Phys. Rev. B 86 (2012) 195106.
[31] F. Birch, Phys. Rev. 71 (1947) 809.
[32] P. Blaha, K. Schwarz, P.H. Dederichs, Phys. Rev. B 37 (1988) 2792.
[33] K. Schwarz, C. Ambrosch-Draxl, P. Blaha, Phys. Rev. B 42 (1990) 2051.
[34] L.A. Errico, M. Rentería, H.M. Petrilli, Phys. Rev. B 75 (2007) 155209.
[35] G.N. Darriba, M. Rentería, H.M. Petrilli, L.V.C. Assali, Phys. Rev. B 86 (2012) 075203.
[36] A.V. Prokofiev, A.I. Shelykh, B.T. Melekh, J. Alloy Compd. 242 (1996) 41.
[37] J.P. McClure, PhD Thesis, University of Nevada, Las Vegas, 2009.
[38] P. Haas, F. Tran, P. Blaha, Phys. Rev. B 79 (2009) 085104.
[39] W.R. Manning, O. Hunter, J. Am. Ceram. Soc. 52 (1969) 492.
[40] K.K. Phani, S.K. Niyogi, J. Am. Ceram. Soc. 70 (1987) C362.
[41] Q. Guo, Y. Zhao, C. Jiang, W.L. Mao, Z. Wang, Solid State Commun. 145 (2008) 250.
[42] D. Lonappan, N.V. Chandra Shekar, P.C. Sahu, B.V. Kumarasamy, A.K. Bandyopadhyay, M. Rajagopalan, Philosop. Mag. Lett. 88 (2008) 473.
[43] L. Bai, J. Liu, X. Li, S. Jiang, W. Xiao, Y. Li, L. Tang, Y. Zhang, D. Zhang, J. Appl. Phys. 106 (2009) 073507.
[44] S. Jiang, J. Liu, X. Li, L. Bai, W. Xiao, Y. Zhang, C. Lin, Y. Li, L. Tang, J. Appl. Phys. 110 (2011) 013526.
[45] K.K. Pandey, N. Garg, A.K. Mishra, S.M. Sharma, J. Phys.: Conf. Series 377 (2012) 012006.
[46] S. Jiang, J. Liu, C. Lin, L. Bai, Y. Zhang, X. Li, Y. Li, L. Tang, H. Wang, Solid State Commun. 169 (2013) 37.
[47] S. Jiang, J. Liu, C. Lin, X. Li, Y. Li, J. Appl. Phys. 113 (2013) 113502.
[48] N.J. Stone, Atom. Data Nucl. Data Tables 90 (2005) 75.
[49] R.D. Shannon, Acta Crystallogr. A 32 (1976) 751.